High-Beta Plasma Confinement and Inward Particle Diffusion in the Magnetospheric Device RT-1

H. Saitoh 1), Z. Yoshida 1), J. Morikawa 1), Y. Yano 1), T. Mizushima 1), Y. Ogawa 1), M. Furukawa 1), K. Harima 1), Y. Kawazura 1), K. Tadachi 1), S. Emoto 1), M. Kobayashi 1), T. Sugiura 1), G. Vogel 1)

1) Graduate School of Frontier Sciences, University of Tokyo, Kashiwa, Chiba, Japan

E-mail contact of main author: saito@ppl.k.u-tokyo.ac.jp

Abstract. High-beta hot-electron plasma is generated and stably sustained in a magnetospheric configuration, the Ring Trap 1 (RT-1) device, generated by a levitated dipole field magnet. Geomagnetic field compensation and optimized operation have realized drastic improvements of the plasma properties. The maximum local beta value has reached 70% and the pressure profiles have rather steep gradient near the superconducting coil. Electrons of high-β plasma consist of typically 70% of hot (~50keV) and the rest of cold populations. Confinement time of the hot component plasma is 0.6s. Inward particle diffusion to the strong field region has been confirmed by pure electron plasma experiment.

1. Introduction

The Ring Trap 1 (RT-1) experiment is a magnetospheric configuration constructed for the confinement of ultra high-β plasma that enables advanced fusion using D-D and D-^{3}He fuels [1,2]. Dipole field is one of the most fundamental magnetic configurations in the Universe, and the goal of RT-1 is to realize high-performance plasma confinement in an artificial magnetosphere. In the magnetospheric configuration, plasma is confined in a dipole field generated by a levitated superconducting magnet [3,4], where the effects of flow and strongly inhomogeneous field play important roles in the confinement and stability properties of the plasma. The mechanism of high-β equilibrium is theoretically explained by the hydrodynamic pressure of fast flow (double Beltrami state) [5-7]. Study of high-β flowing plasma is important for understanding the fundamental physics of self-organization of magnetized charged particles, as well as for the realization of advanced fusion concept.

RT-1 succeeded to generate its first plasma in 2006, and in the first series of experiments, plasma is generated and sustained by electron cyclotron resonance heating (ECH) with 8.2 and 2.45 GHz microwaves [8-12]. Although ions are not directly heated at present, we can conduct magnetohydrodynamically equivalent experiment on magnetospheric plasma using hot-electron plasma generated by ECH. In this study, we report the experimental results of the improved high-β ECH plasma in RT-1 realized by the optimization of plasma formation operation and compensation of the geomagnetic field [13]. The maximum local β value reached 70%, and particle confinement time is approximately 0.6s in the most recent experiment in RT-1. The plasma pressure is mainly resulted from hot electrons and has a peak in the strong field region, which spatial profiles of soft x-ray radiation were observed by a CCD camera [14]. Fluctuation-induced particle diffusion into the strong field region was confirmed by experiments with pure electron plasma [3].

2. Experimental Setup and Recent Progress

Figure 1 shows cross sections of RT-1 and visible light CCD camera image of the plasma. Inside the chamber, RT-1 has a dipole field magnet made with Bi-2223 high-temperature

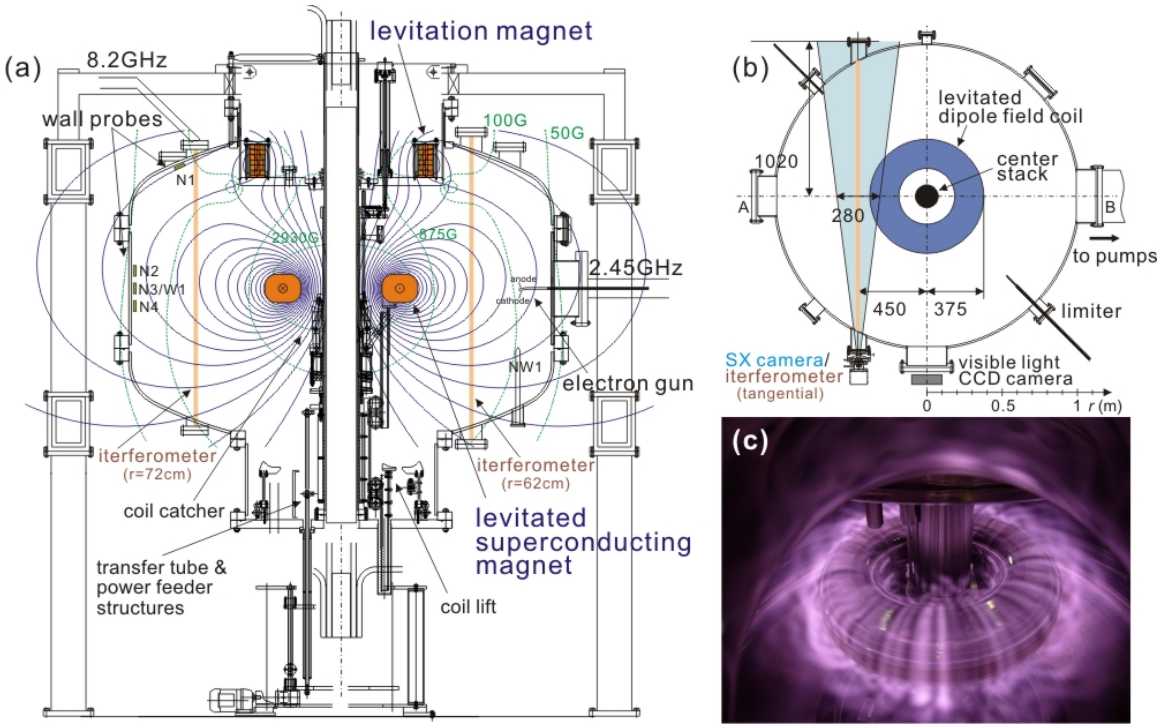

FIG. 1. (a) Cross section and (b) top view of RT-1 including vacuum chamber, coil magnets and diagnostics. (c) Visible light image of magnetospheric plasma generated in RT-1.

superconducting wires that generates a magnetosheric dipole field. In order to minimize perturbations to the plasma, the superconducting magnet of RT-1 is operated with a permanent current mode and magnetically levitated by a feedback-controlled normal-conducting levitation electromagnet located at the top of the chamber [10,12]. The superconducting and levitation coils are operated with 250kA and 28.8kA. The combination of two magnets generates separatrix configuration as shown in Fig.1 (a), and the plasma is separated from the chamber wall in the vacuum field. The dipole field coil is cooled down to 20K using three GM refrigerators, and we conduct 6 hours of plasma experiment before the coil temperature rises to 30K. In order to improve the accuracy of geomagnetic field compensation, the correction coils were replaced with a new system in 2008 [13]. The available microwave powers are up to 25kW (1s) at 8.2GHz and up to 20kW (2s) at 2.45GHz at present. The working gases are hydrogen and helium, which are continuously introduced into the vacuum chamber through a piezo valve located at the bottom of chamber. Detailed descriptions on the RT-1 device are presented in [11].

Diagnostic system of RT-1 is as follows: Plasma diamagnetism is measured by four magnetic loops winded outside of the chamber and multi-channel hall probes installed inside the chamber. Equilibrium pressure profiles are estimated by using Grad-Shafranov analysis based on the magnetic measurements. We found an empirical relation between the averaged diamagnetic signal $\Delta\Phi$ and the maximum local β: $\beta[\%]\sim18\times\Delta\Phi[\mathrm{mWb}]$ in the present plasma pressure range. A 75GHz (4mm) microwave interferometer is used to measure the line integrated electron density. Transmitting and receiving antennas of the interferometer were positioned at vertical ports at r=62 or 72cm (Fig.1a), or tangential ports (Fig.1b). We compared the interferometer data for similar conditions in different experiment, and estimated the density profiles of the plasma. For relatively low density plasma, we also used an edge Langmuir probe for the measurements of electron density and temperature profiles. For the measurements of bremsstrahlung x-ray energy distribution, Si(Li) detectors and pulse height

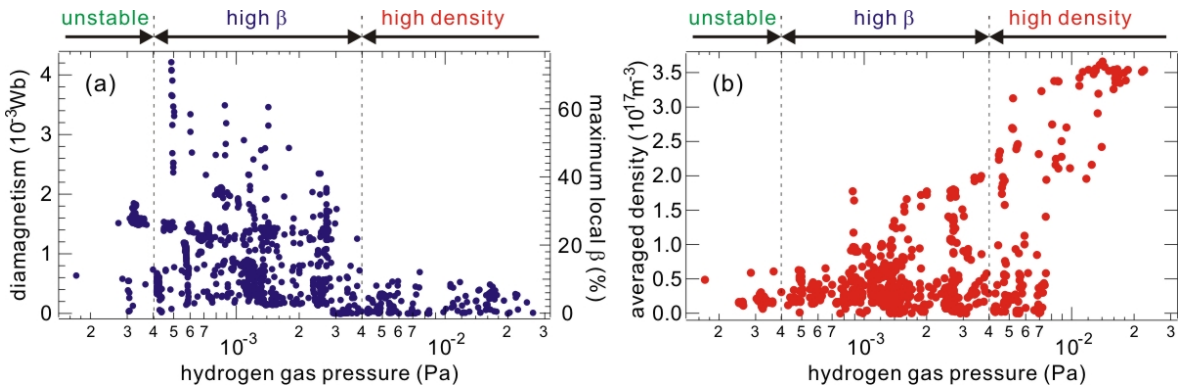

FIG. 2. (a) Diamagnetic loop signal (averaged value of four loops and estimated maximum local β) and (b) line averaged electron density, in the variation of neutral gas pressure.

analysis (PHA) systems were used in order to determine the hot electron temperature and line integrated density. An x-ray pinhole camera [14] with a 1024×1024 pixel 16bit dynamic range CCD was used for imaging x-ray strength (Fig.1b). The x-ray camera can be used for the measurement of electron temperature by photon counting mode. Plasma fluctuations are measured by diamagnetic pickup coils, Langmuir probes, and the interferometer.

3. Improved High-Beta Stable State

Plasma in high-β and high-density states is generated depending on the filled neutral gas pressure P_n and injected microwave power P_f. Figure 2 shows diamagnetism ΔΨ and line averaged density n_e in variation of P_n. ΔΨ is an averaged signal of four magnetic loops, and n_e is inferred from measurements of interferometer located at the tangential port. The maximum local β of the plasma estimated from Grad-Shafranov numerical calculation is also shown in Fig.2 (a). The parameter ranges are designated as *high-density*, *high-β*, and *unstable* modes depending on P_n as shown in the figure. The highest electron density is realized at 4mPa<P_n, but the plasma has relatively low β in this pressure range. High β plasma is realized in pressure range ~0.4-4mPa, which is characterized by large stored energy, strong x-ray radiation, and depression of visible light strength and fluctuation levels. When P_n is lower than approximately 0.4mPa, the plasma is unstable as described in the following sections, and it has rather low diamagnetic pressure and number density. In ECH experiments in RT-1 carried out so far, plasma pressure is mainly resulted from hot electrons, and the highest β was realized by increasing the input RF power and lowering P_n close to the unstable range.

Temporal evolution of high β plasma formation is shown in Figure 3 (a)-(d). The plasma was generated with applied RF power of 20kW at 2.45GHz and 25kW at 8.2GHz both injected from t=0 to 1s at P_n=0.5mPa. At this neutral gas pressure, there is a time lag between the start of microwave injection and high density plasma formation. The time lag is lengthened and stable high β discharge is difficult to sustain by decreasing P_n. (i) From t=0 to 0.46s, very low density (typically ~10^{15}m^{-3}) plasma was generated with strong x-ray radiation, suggesting thin plasma consists of extremely hot electrons. Microwave at 2.45GHz was not effectively absorbed in this period. (ii) The reflection power gradually decreased during continuous microwave injection, and jump to high density state was observed at t=0.46s accompanied with rapid increase in visible light strength. Then, strength of visible light dropped rapidly and the stored energy started to increase. (iii) After the increase in stored energy saturated, high β stable state was realized. In the data shot presented in Fig.3, the maximum local β is calculated to be 70%, and the pressure peak was located at r=49cm on the z=0cm plane. The

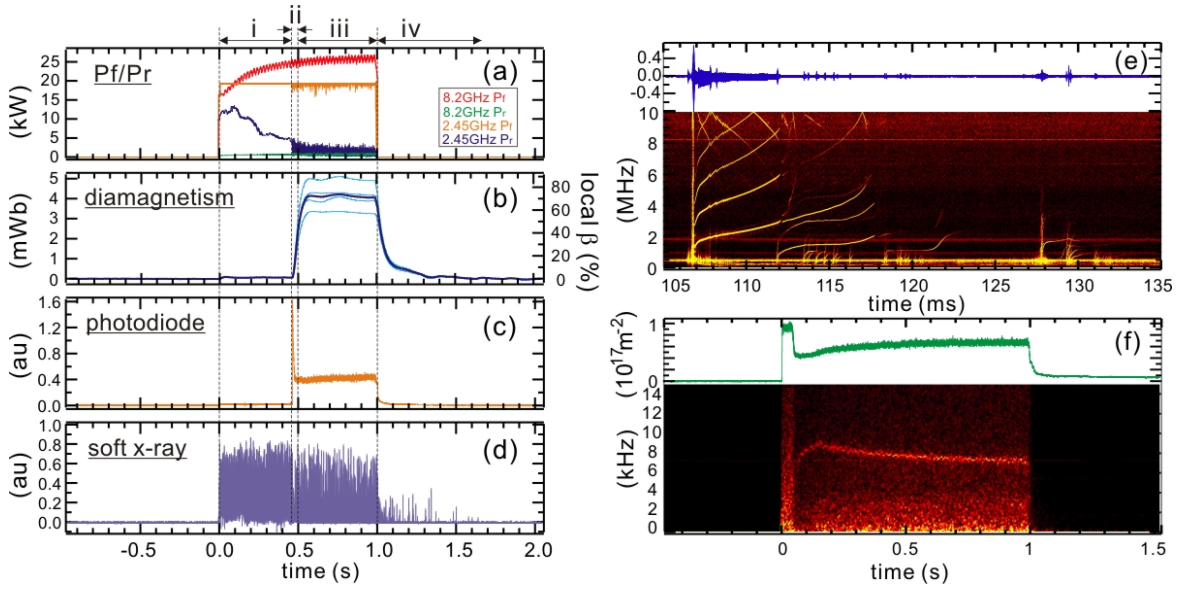

FIG. 3. (a)-(d) Typical waveforms of high-β (local β~70%) plasma formation. Fluctuations and its power spectrum (e) measured by a magnetic probe in low-density and extremely hot electron mode (phase i of Fig.3 (a)) and (f) measured by an interferometer in a different condition.

plasma had a typical density of 10^{17}m^{-3} in this phase. (iv) After microwaves were turned off at t=1s, plasma density and diamagnetic signal decayed slowly in afterglow phase.

Figure 3 (e) shows chirping of magnetic fluctuations measured by a pickup coil in phase (i) of another discharge with similar conditions. After the onset of instability at t=105.6ms, lowest mode frequency ascended from 0.5 to 3MHz. The frequency sweep rate was correlated with conditions of plasma formation, and faster chirp was observed by increasing P_f and decreasing P_n. After t=112ms, rapid growth and decay of fluctuation and frequency sweep were repeatedly observed. In this phase, the fluctuation amplitude tends to decay with saturation of frequency sweeping. These high frequency modes are stabilized after the formation of high density plasma and were not observed in phase (iii). When P_n is lower than approximately 0.4mPa, however, rapid decrease in β and n_e, or plasma disruption, was sometimes observed during high density state with the onset of instability. Figure 3 (f) shows another low frequency fluctuation mode measured by a 75GHz interferometer. This fluctuation has a coherent mode structure, and its frequency tends to decrease with increasing n_e. The same fluctuation was also observed by a reflectometer, magnetic probes, and Langmuir probes. The characteristics of the high and low frequency fluctuations are similar to electrostatic modes observed in LDX [15]. The effects of hot electrons are possible reasons for the onset of instability, though further investigation is needed to identify the observed fluctuation modes.

4. Properties of Hot Electron Plasma and Confinement Time

Figure 4 shows typical visible light and x-ray images of ECH plasma observed at a tangential port (Fig.1b). When 8.2 GHz microwave was applied, where the ECR layer (0.293T) intersects the superconducting coil case, the strong x-ray emitting region was localized near the superconducting coil. Bremsstrahlung on the coil case was also observed, indicating that some of the hot electrons were lost before filling the confinement region. Clear spatial dependence in electron temperatures was not observed. When the superconducting coil was not levitated, strong x-ray radiation was observed at the support structure, indicating that it was a major loss route of hot electrons.

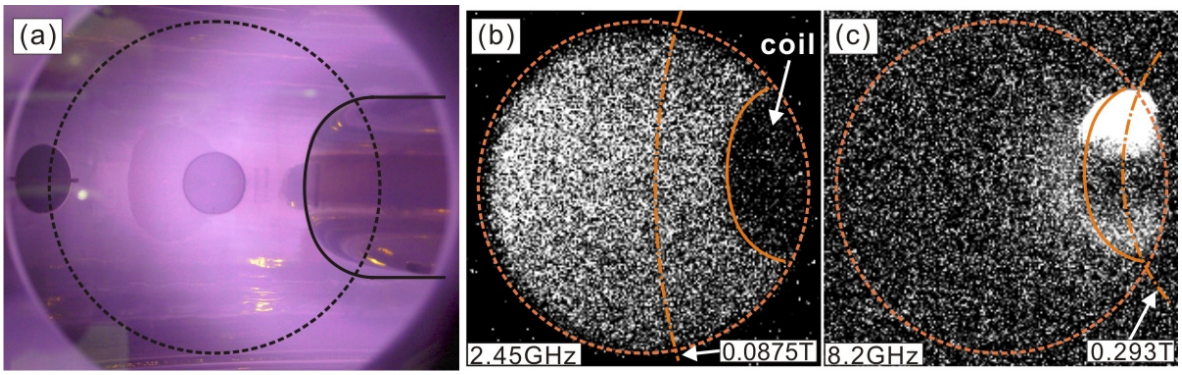

FIG. 4. (a) Visible light image and typical x-ray images of plasmas generated by (b) 2.45GHz and (c) 8.2GHz ECH. Dotted line show field of view of the x-ray camera.

Figure 5 (a) shows temperature T_h and density n_h of hot electrons measured by a Si(Li) detector. Plasma was generated by injecting 5kW of 2.45GHz RF in variation of P_n. Assuming a Maxwellian energy distribution of hot electrons, bremsstrahlung photon number dN/dE_x due to interaction between free electrons and ions is proportional to $n_h n_i Z_{eff}^2 \exp(-E_x/T_h)/E_x T_h^{0.5}$, where Z_{eff} is the effective charge and E_x is photon energy [16]. T_h was estimated from PHA data of the detector by the curve fitting method to dN/dE_x including the effects of the transmittance of a Be window and photon efficiency of the Si(Li) detector. Then T_h was used to determine n_h, supposing that plasma consists of hydrogen ions and taking plasma volume and detection angle into account. By decreasing P_n, increase in T_h and n_h was observed. $P_h=n_hT_h$ was consistent with the diamagnetic measurements when hot electrons were major component of electrons. Strong correlation between P_h and diamagnetism (Fig.5b) also indicates that plasma pressure is mainly resulted from hot electrons in such cases.

Soft x-ray measurements using Si(Li) detectors show that the hot electron component is in the temperature range of ~1-50keV. Edge Langmuir probe measurements show that plasma also has cold electrons around ~10eV. The hot electron component has relatively long confinement time due to its small cross section of collisions. Decay of electron line density after microwave was turned off is shown in Fig.6 (a). The decay curve has two different time constants, corresponding to hot and cold components of electrons. Fig.6 (c) and (d) shows the ratio of slow decay component of density, and time constants of fast and slow decay measured by double exponential fitting of the decay curve. By optimizing neutral gas pressure, increase in the ratio of hot component and decay time was observed. The maximum confinement time of plasma density was τ_p=0.6s. Diamagnetic measurements showed that energy confinement

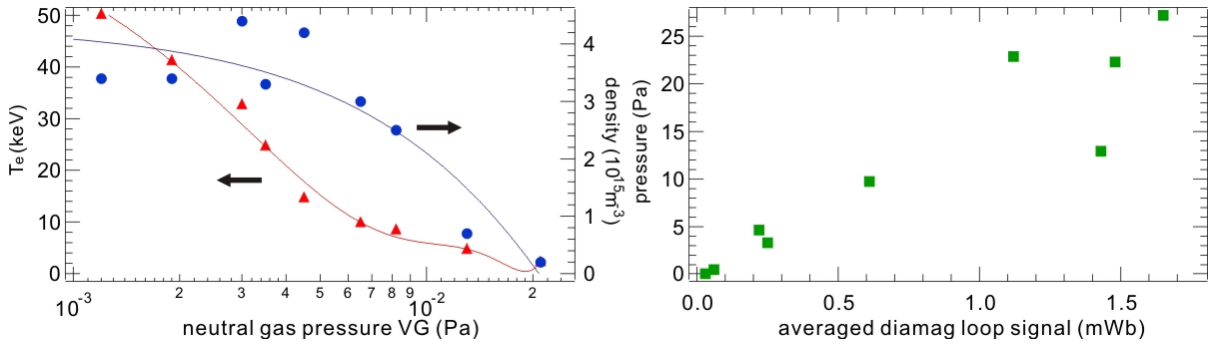

FIG. 5. (a) Temperature T_h (triangles) and density n_h (circles) of hot electrons in the variation of filled neutral gas. (b) Hot electron pressure $P_h=n_hT_h$ in the variation of diamagnetic signal.

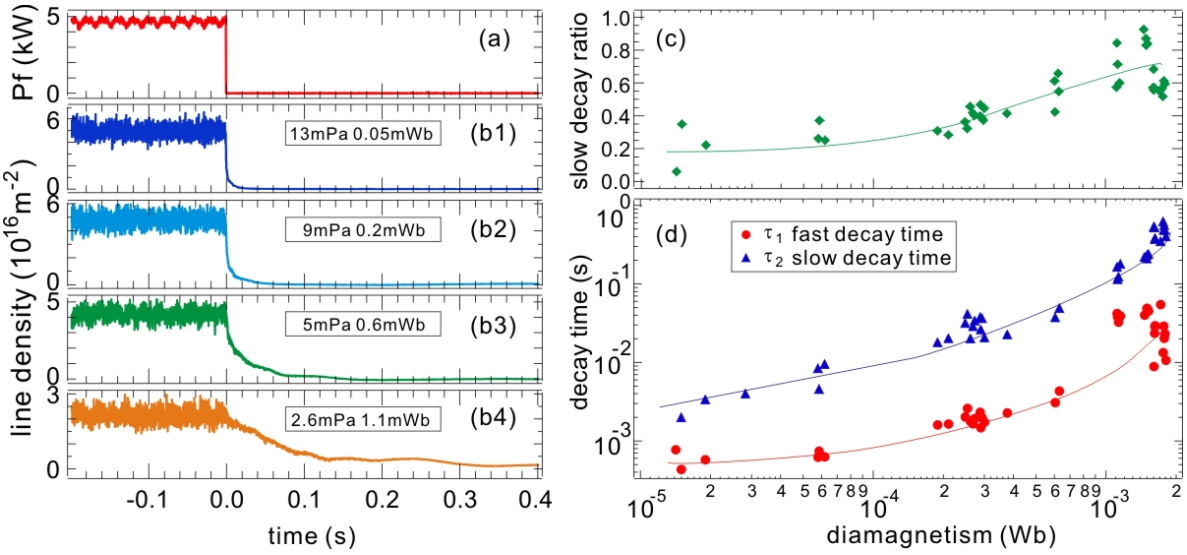

FIG.6. (a) Injection power of 2.45GHz microwave and (b) temporal decay of line density after the termination of microwave at t=0s with different neutral gas pressures. (c) Ratio of slow decay component electrons and (d) time constants of decay times in variation of neutral gas pressure.

time τ_e was comparable to τ_p. It suggests that temporal variation of T_h in the afterglow phase was relatively small, and it is consistent with soft x-ray measurements in the afterglow phase. Using typical parameters T_h=50keV, n_e=10^{17}m^{-3}, B=0.1T in the core region, and plasma radius r_p=0.3m, Bohm and classical diffusion times are calculated to be τ_B~1.4μs and τ_c=3.0×10^3s, and we have τ_p~4×10^5 τ_B and τ_p~2×10^{-4} τ_c.

5. Peaked Density Profiles and Inward Diffusion of Particles

Radial density profiles of the plasma were estimated from multiple cord measurements of the 75GHz interferometer. Because the interferometer has only 1ch, simultaneous multi-cord measurements were not carried out at present. Electron line density n_l was repeatedly measured at different cords in similar plasma formation conditions with good reproducibility. The horn antennas of the interferometer were set at tangential ports at y=45cm or vertical ports at r=62 or 72cm. The light path of the tangential cord is close to the dipole field coil, while those of vertical ports are rather close to the chamber wall (Fig.1). We estimated the radial profile of plasma assuming that electron density is a function of magnetic surface Ψ=rA_θ and it has power-low dependence on r on the equator (z=0cm) plane of the chamber,

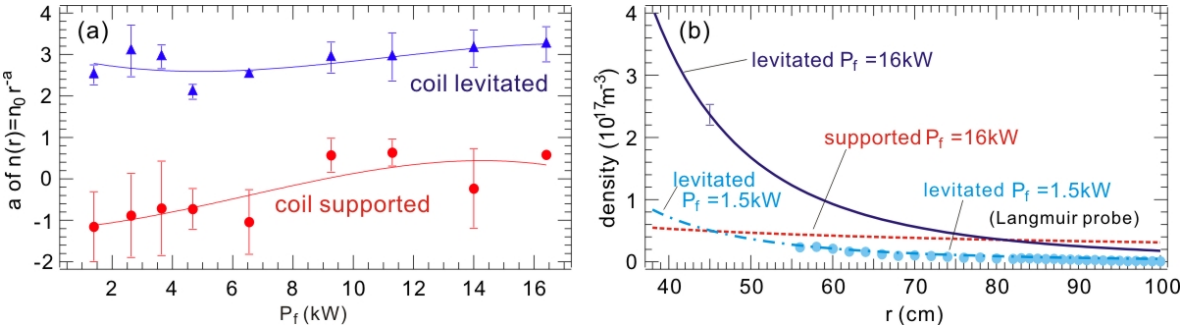

FIG. 7. (a) Coefficient a of Eq.1 with and without coil levitation in variation of 2.45GHz RF power. (b) Radial electron density profiles inferred from measurements of the interferometer. Measurements with a Langmuir probe are also shown for comparison for small P_f.

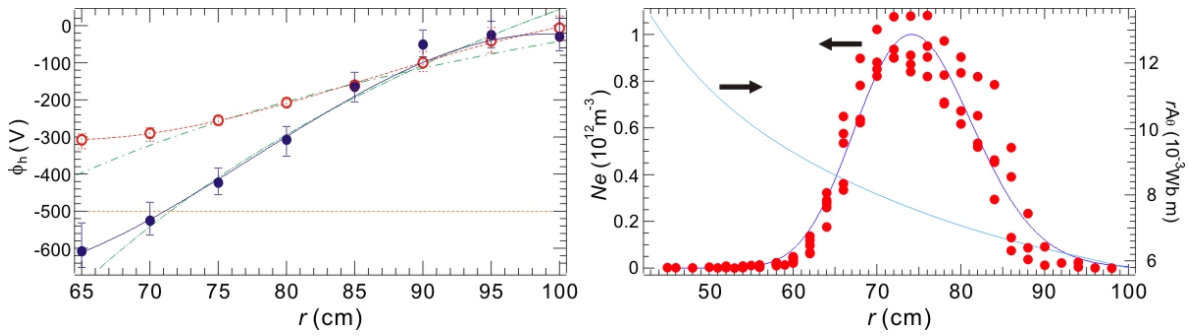

FIG. 8. (a) Radial profiles of electrostatic potential with (closed circle) and without (open circles) coil levitation, and (b) radial profile of electron density, of non-neutral (pure electron) plasma.

$$n(r) = n_0 r^{-a}. \quad (1)$$

Figure 7 (a) shows coefficient a of Eq.1 for various P_f of 2.45GHz microwave with and without coil levitation. When not levitated, the dipole field coil was operated at 90% of its rated current, so that the shapes of the magnetic surfaces in both cases were quite similar. Thus, variation in plasma properties is attributed solely to the effects of the coil support structure. By coil levitation, drastic increase in n_l was observed in the measurement at the tangential cord, indicating the increase in n_e in a strong field region. As shown in Fig.7 (a), a=-0.3±0.7 when the coil was not levitated, and a=2.8±0.4 when levitated. The solid and dotted lines in Fig.7 (b) show the estimated n_e profiles when P_f=16kW with and without coil levitation. By removing perturbations due to the coil support structure, peaked density profile is realized [4]. When P_f is small, an edge Langmuir probe can be used for the measurement of radial n_e profiles. The chain line in Fig.7 (b) show n_e profiles measured by the interferometer when P_f=1.5kW with coil levitation, which shows good agreement with that of the Langmuir probe at the edge region, plotted as closed circles in the figure.

Inward diffusion of charged particles in the magnetospheric configuration was also observed in experiments with pure electron plasma. In RT-1, toroidal non-neutral plasma consists of only electrons is stably trapped for more than 300s [3]. Figure 8 (a) shows high-impedance potential profiles of the electron plasma during beam injection. The electron gun was located at r=70cm and electrons were injected with initial acceleration voltage of V_{acc}=500V. When the coil was levitated, toroidal E×B drift speed was close to rigid-rotor motion especially near the electron gun, but it had some remaining differential motion during beam injection. Figure 8 (b) shows the density profile of electron plasma during beam injection. Electrons were injected from the gun located at r=80cm. Electrons were observed to be transported from the initial magnetic surface and the density peak shifted inward. In a stable confinement phase after beam injection ended, measurements with multiple wall probes [17] showed that plasma is confined in a strong field region. In this phase, electrostatic fluctuation of the plasma had peaked frequency spectrum. These observations strongly suggest the spontaneous formation of a rigid-rotor stable equilibrium state of non-neutral plasma in the magnetospheric configuration. In RT-1, the plasma has large electrostatic fluctuation in the diocotron (Kelvin-Helmholtz) [18] frequency range during electron injection, which can cause radial penetration of electrons breaking conservation of the third adiabatic invariant.

Inward pinch of charged particles in a magnetospheric configuration was theoretically predicted by Hasegawa [1,2]. He pointed out that plasma satisfies $\partial f/\partial\Psi$=0 in a stable equilibrium state, where there is no driving force of drift wave turbulence. Here $f(\mu, J, \Psi)$ is

the phase space density as a functions of the adiabatic invariants, and turbulent-induced diffusion occurs until the plasma density per flux tube becomes constant. In the strongly inhomogeneous dipole field, the stable condition requires strongly peaked density profiles in the strong field region. Observation of the inward diffusion and self organization of stable vortex structures [3,4] are consistent with the predicted turbulent-induced pinch, and it is one of the fundamental mechanisms of relaxation process in the magnetospheric configuration.

Acknowledgements

This work was supported by Grants-in-Aid for Scientific Research (14102033 and 19340170) from Ministry of Education, Sports, Culture, Science and Technology of Japan.

REFERENCES

[1] HASEGAWA, A, "Dipole field fusion reactor", Comm. Plasma Phys. Controlled Fusion **11** (1987) 147.
[2] HASEGAWA, A., et al., "A D-^{3}He fusion reactor based on a dipole magnetic field", Nucl. Fusion **30** (1990) 2405.
[3] YOSHIDA, Z., et al., "Magnetospheric vortex formation: Self-organized confinement of charged particles", Phys. Rev. Lett. **104** (2010) 235004.
[4] BOXER, A.C., et al., "Turbulent inward pinch of plasma confined by a levitated dipole magnet", Nature Phys. **6** (2010) 207.
[5] MAHAJAN, S.M. and YOSHIDA, Z., "Double curl Beltrami flow: Diamagnetic structures", Phys. Rev. Lett. **81** (1998) 4863.
[6] YOSHIDA, Z. and MAHAJAN, S.M., "Variational principles and self-organization in two-fluid plasmas", Phys. Rev. Lett. **88** (2002) 095001.
[7] SHIRAISHI, J., et al., "Relaxation of a quasisymmetric rotating plasma: A model of Jupiter's magnetosphere", Phys. Plasmas **12** (2005) 092901.
[8] YOSHIDA, Z., et al., "First plasma in the RT-1 device", Plasma Fusion Res. **1** (2006) 008.
[9] YOSHIDA, Z., et al., "RT-1 project: magnetosphere-like plasma experiment", Fusion Sci. Tech. **51** (2007) 29.
[10] MORIKAWA, J., et al., "Development of a super-conducting levitated coil system in the RT-1 magnetospheric configuration device", Fusion Eng. Design **82** (2007) 1437.
[11] OGAWA, Y., et al., "Construction and operation of an internal coil device, RT-1, with a high-temperature superconductor", Plasma Fusion Res. **4** (2008) 020.
[12] YANO, Y., et al., "Feedback control of the position of the levitated superconducting magnet in the RT-1 device", Fusion Eng. Design **85** (2010) 641.
[13] YANO, Y., et al., "Improvement of field accuracy and plasma performance in the RT-1 device", Plasma Fusion Res. **4** (2009) 039.
[14] SAITOH, H., et al., "Initial results of x-ray imaging and energy spectrum measurements of hot electron plasmas in RT-1", Plasma Fusion Res. **4** (2009) 050.
[15] GARNIER, D.T., et al., "Production and study of high-beta plasma confined by a superconducting dipole magnet", Phys. Plasmas **13** (2006) 056111.
[16] HUTCHINSON, I.H., Principles of Plasma Diagnostics, Cambridge University Press, Cambridge (2002).
[17] SAITOH, H., et al., "Measurement of the density profile of a toroidal non-neutral plasma by a wall-probe array", Plasma Fusion Res. **4** (2009) 054.
[18] LEVY, R.H., et al,. "Ion resonance instability in grossly nonneutral plasmas", Phys. Fluids **12** (1969) 2616.